CHIN.PHYS.LETT. Vol. 19, No. 1 (2002) 83

Effects of Particle Size on Dilute Particle Dispersion in a Kármán Vortex Street Flow *

WU Zuo-Bing(武作兵)[1], LING Guo-Can(凌国灿)[1], XING Qi-Jiang(邢启江)[2]
[1]*State Key Laboratory of Nonlinear Mechanics, Institute of Mechanics, Chinese Academy of Sciences, Beijing 100080*
[2]*Department of Physics, Peking University, Beijing 100871*

(Received 5 June 2001)

It is shown that in a Kármán vortex street flow, particle size influences the dilute particle dispersion. Together with an increase of the particle size, there is an emergence of a period-doubling bifurcation to a chaotic orbit, as well as a decrease of the corresponding basins of attraction. A crisis leads the attractor to escape from the central region of flow. In the motion of dilute particles, a drag term and gravity term dominate and result in a bifurcation phenomenon.

PACS: 47.52.+j

The motion of bubbles, drops and solid particles in a non-uniform flow has received great attention due to its applications and fundamental significance. It plays a dominant role in the transport phenomena of particulate and multi-phase systems. Due to particle motion in the low Reynolds number category, the equation of motion for a small rigid sphere in a non-uniform flow filed is deduced.[1] The motion of particles has abundant phenomena, even though the background flow is very simple. Especially, when the background flow is dominated mainly by large-scale structures, the fluid viscosity is not included in the governing flow equation.[2] In a periodic Stuart vortex flow, depending on the value of parameters, the particles asymptotically concentrate along periodic, quasi-periodic, or chaotic open trajectories.[3,4]

For the particle dispersion in a plane wake flow, the particle focusing is shown experimentally and studied by discrete vortex methods.[5] In the range of the Reynolds number, the plane wake flow can be modelled by a Kármán vortex street. By considering Stokes drag, this focusing phenomenon is studied in terms of the two-dimensional central manifolds.[6] In the Lagrangian motion equation of dilute particles, dimensionless parameters closely join together, for example, particle size is related to the parameters, which cannot be taken as continuous dynamical parameters when the others are constants. In this letter, we will consider the effects of particle size on dilute particle dispersion in a Kármán vortex street flow.

The motion of a small spherical particle in a non-uniform flow field $\boldsymbol{u}$ is governed by the momentum equation[1,4]

$$\frac{\pi}{6}d_{\rm P}^3(\rho_{\rm P}+0.5\rho_F)\frac{{\rm d}\boldsymbol{V}}{{\rm d}t}=\frac{\pi}{6}d_{\rm P}^3(\rho_{\rm P}-\rho_{\rm F})\boldsymbol{g}+\frac{\pi}{4}d_{\rm P}^3\rho_{\rm F}\frac{D\boldsymbol{u}}{Dt}+3\pi d_{\rm P}\nu\rho_{\rm F}(\boldsymbol{u}-\boldsymbol{V})f_d+\frac{3}{2}(\pi\nu)^{1/2}d_{\rm P}^2\rho_{\rm F}\int_0^t\frac{1}{\sqrt{t-\tau}}\cdot\left(\frac{{\rm d}\boldsymbol{u}}{{\rm d}\tau}-\frac{{\rm d}\boldsymbol{V}}{{\rm d}\tau}\right){\rm d}\tau+\frac{\pi}{12}d_{\rm P}^3\rho_{\rm F}(\boldsymbol{u}-\boldsymbol{V})\times\boldsymbol{\omega},\quad(1)$$

where $\boldsymbol{V}$ is the velocity of the particle, $d_{\rm P}$ is the particle diameter, ρ is the density, $\boldsymbol{g}$ is the gravitational acceleration, ν is the fluid kinematic viscosity, $\boldsymbol{\omega}$ is the vorticity of the flow fluid, and the subscripts F and P refer to the fluid and particle, respectively. The parameter f_d related to the Reynolds number ($R_{\rm P}=|\boldsymbol{u}-\boldsymbol{V}|d_{\rm P}/\nu$) is described[7,4] as

$$f_d=1+0.1315R_{\rm P}^{0.82-0.05\log_{10}R_{\rm P}},\quad 0<R_{\rm P}<200.\quad(2)$$

Introducing the dimensionless quantities $\delta=\rho_{\rm P}/\rho_{\rm F}$, $\epsilon=1/(0.5+\delta)$, $t^*=t/T$, $\boldsymbol{V}^*=\boldsymbol{V}/(l/T)$, $\boldsymbol{u}^*=\boldsymbol{u}/U_\infty$, $\boldsymbol{\omega}^*=\boldsymbol{\omega}l/U_\infty$, and $\boldsymbol{g}^*=\boldsymbol{g}/g$ (T is the particle viscous relaxation time $d_{\rm P}^2/(18\epsilon\nu)$), we non-dimensionlize Eq. (1) and ignore the Basset history term. Thus, Eq. (1) can be described by

$$\frac{{\rm d}\boldsymbol{V}}{{\rm d}t}=B\boldsymbol{g}+\frac{3}{2}\epsilon A^2\boldsymbol{u}\cdot\nabla\boldsymbol{u}+(A\boldsymbol{u}-\boldsymbol{V})f_d+\frac{1}{2}\epsilon A(A\boldsymbol{u}-\boldsymbol{V})\times\boldsymbol{\omega},\quad(3)$$

where $A=U_\infty T/l$, $B=(1-1.5\epsilon)T^2g/l$ and the asterisks for the dimensionless quantities are omitted for convenience. Moreover, the Reynolds number is written as $R_{\rm P}=\overline{R}_{\rm P}/A|A\boldsymbol{u}-\boldsymbol{V}|$ ($\overline{R}_{\rm P}=U_\infty d_{\rm P}/\nu$).

The flow field $\boldsymbol{u}$ is chosen to be a Kármán vortex street flow. Since the size of particles and their concentration are sufficiently small, their mutual interactions as well as their effects on the base flow can be neglected. The stream function of Kármán vortex street flow is

$$\Psi(x,y)=\frac{\Gamma}{4\pi}\ln\frac{{\rm ch}[2\pi(y-h/2)/l]-\cos(2\pi x/l)}{{\rm ch}[2\pi(y+h/2)/l]+\cos(2\pi x/l)}+v_cy,\qquad v_c=\frac{\Gamma}{2l}{\rm th}\frac{\pi h}{l},\quad(4)$$

where Γ is the strength of vortices, l and h are the streamwise and transverse spacing of vortices, respec-

*Supported in part by the National Key Programme for Developing Basic Science G1999032801-11, the Innovation Programme of Chinese Academy of Sciences, and the Climbing A Pre-Selected Project.

tively. The dimensionless quantities denoted by asterisks are defined as $x^* = x/l$, $y^* = y/l$, $h^* = h/l$, $\Gamma^* = \Gamma/(U_\infty l)$ and $\Psi^* = \Psi/(U_\infty l)$. A parameter κ is introduced to remove the singularities of the velocity field $\boldsymbol{u}$ [6] and the asterisks for the dimensionless quantities are omitted for convenience. Thus, the modified velocity field is given by

$$\begin{aligned} u_x &= \frac{\partial \Psi}{\partial y} = \frac{\Gamma}{2}\left[\frac{\mathrm{sh}[2\pi(y-h/2)]}{\mathrm{ch}[2\pi(y-h/2)] - \kappa\cos(2\pi x)}\right. \\ &\quad \left. - \frac{\mathrm{sh}[2\pi(y+h/2)]}{\mathrm{ch}[2\pi(y+h/2)] + \kappa\cos(2\pi x)}\right] + v_c, \\ u_y &= -\frac{\partial \Psi}{\partial x} = -\frac{\Gamma\kappa}{2}\left[\frac{1}{\mathrm{ch}[2\pi(y-h/2)] - \kappa\cos(2\pi x)}\right. \\ &\quad \left. + \frac{1}{\mathrm{ch}[2\pi(y+h/2)] + \kappa\cos(2\pi x)}\right]\sin(2\pi x), \end{aligned} \tag{5}$$

which has the symmetries

$$\begin{aligned} &u_x(x,-y,-\kappa) = u_x(x,y,\kappa), \\ &u_y(x,-y,-\kappa) = u_y(x,y,\kappa), \\ &u_x(x+1/2,-y,\kappa) = u_x(x,y,\kappa), \\ &u_y(x+1/2,-y,\kappa) = u_y(x,y,\kappa). \end{aligned}$$

Only when $\kappa = 1$, does the velocity field satisfy the Euler equation. Since the error increases with the deviation of κ from 1, we take $\kappa = 0.99$ as an approximation in this simulation.

The particle motion is described by a four-dimensional, nonlinear autonomous dynamical system of the form

$$\begin{aligned} \dot{x} &= V_x, \quad \dot{y} = V_y, \\ \dot{V}_x &= \frac{3}{2}\epsilon A^2 \boldsymbol{u}\cdot\nabla u_x + (Au_x - V_x)f_d \\ &\quad + \frac{1}{2}\epsilon A\omega_z(Au_y - V_y), \\ \dot{V}_y &= \frac{3}{2}\epsilon A^2 \boldsymbol{u}\cdot\nabla u_y + (Au_y - V_y)f_d \\ &\quad - \frac{1}{2}\epsilon A\omega_z(Au_x - V_x) - B. \end{aligned} \tag{6}$$

Using a fourth-order Runge–Kutta algorithm, we integrate Eqs. (6) with a time step $\Delta t = 0.01$. Since air is chosen as the fluid media in the wake, the properties of fluid in Eqs. (6) are $\rho_F = 1.225\,\mathrm{kg/m^3}$ and $\nu = 1.45 \times 10^{-5}\,\mathrm{m^2/s}$.[8] Moreover, other parameters in Eqs. (6) can be taken as $U_\infty = 4\,\mathrm{m/s}$, $\rho_\mathrm{P} = 2.4\times10^3\,\mathrm{kg/m^3}$ from Ref. [5] as well as $\Gamma = 1$ and $h = 0.3$. In order to draw a bifurcation diagram and particle trajectories, 20 points along the y coordinate and 100 points in the street with their corresponding flow field velocities are taken as initial conditions of Eqs. (6), respectively. We investigate the motion of particles under the variation of d_P for $l = 0.1\,\mathrm{m}$. In the total 21 000 time steps, points in the first 20 000 time steps are discarded as transients; points in the following 1000 time steps are plotted as particle trajectories. In the particle trajectories, points y at $x = 0$ versus d_P are plotted as a bifurcation diagram. For a dense bifurcation zone, the diagram is calculated again by using a smaller time step $\Delta t = 0.001$ and enlarged.

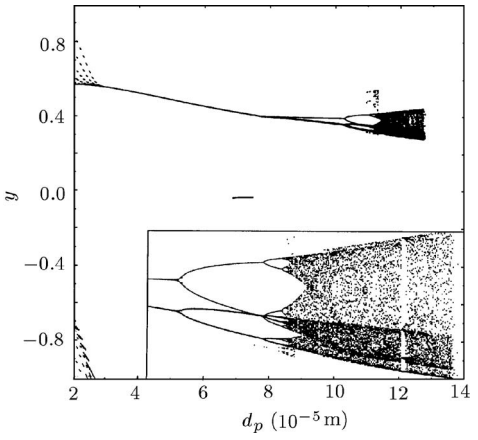

Fig. 1. A bifurcation diagram for a continuous range of d_P showing the vertical position of particles at $x = 0$. The dense bifurcation zone is enlarged and redrawn at the bottom-right corner.

In order to display the influence of particle size on the dilute particle dispersion, we plot a bifurcation diagram $y \sim d_\mathrm{P}$ in Fig. 1. When $d_\mathrm{P} < 2.62 \times 10^{-5}\,\mathrm{m}$, the velocity of the particle dispersion is very slow, so that most of the particle trajectories are preserved near the street, as well as divided into two sets: one above the street, the other under the street. When $d_\mathrm{P} \geq 2.62 \times 10^{-5}\,\mathrm{m}$, particle trajectories under the street leave far from the street, but the particle trajectories above the street converge on a period-1 orbit. For $d_\mathrm{P} = 2.62\times10^{-5}\,\mathrm{m} - 7.85\times10^{-5}\,\mathrm{m}$, period-1 orbits above the street are presented as particle trajectories. Especially, for $d_\mathrm{P} = 6.87 \times 10^{-5}\,\mathrm{m} - 7.48 \times 10^{-5}\,\mathrm{m}$, another period-1 orbit appears in the street. In this case, there are two attractors for the particle trajectories. As $d_\mathrm{P} = 7.85 \times 10^{-5}\,\mathrm{m}$, the period-1 orbit bifurcates to a period-2 orbit. For $d_\mathrm{P} = 7.85 \times 10^{-5}\,\mathrm{m} - 1.03 \times 10^{-4}\,\mathrm{m}$, particle trajectories are presented as period-2 orbits. As $d_\mathrm{P} = 1.03 \times 10^{-4}\,\mathrm{m}$, the period-2 orbit bifurcates to a period-4 orbit. For $d_\mathrm{P} = 1.03\times10^{-4}\,\mathrm{m} - 1.10\times10^{-4}\,\mathrm{m}$, particle trajectories converge on period-4 orbits. When $d_\mathrm{P} > 1.10 \times 10^{-4}\,\mathrm{m}$, the period-4 orbit bifurcates further to a period-8 orbit and finally to a quasi-periodic or chaotic orbit. This bifurcation behaviour is clearly presented in the enlarged zone in Fig. 1. As $d_\mathrm{P} = 1.276 \times 10^{-4}\,\mathrm{m}$, a crisis occurs, so that the quasi-periodic or chaotic orbit disappears, i.e. escapes from the central region of flow. Moreover, a similar bifurcation process emerges in a range near $d_\mathrm{P} = 1.1 \times 10^{-4}\,\mathrm{m}$.

In the following, we give some examples for different values of d_P. In order to display the dispersion of particles in the street, we also plot the basin of attraction in Fig. 3, which describes a distribution of initial

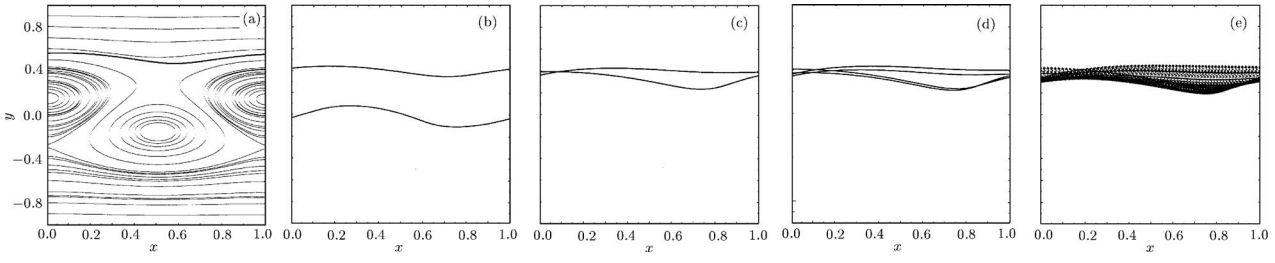

Fig. 2. Typical trajectories on the $x-y$ plane for: (a) $d_{\rm P}=3\times10^{-5}$ m and all streamlines; (b) $d_{\rm P}=7\times10^{-5}$ m; (c) $d_{\rm P}=1\times10^{-4}$ m; (d) $d_{\rm P}=1.05\times10^{-4}$ m; (e) $d_{\rm P}=1.2\times10^{-4}$ m.

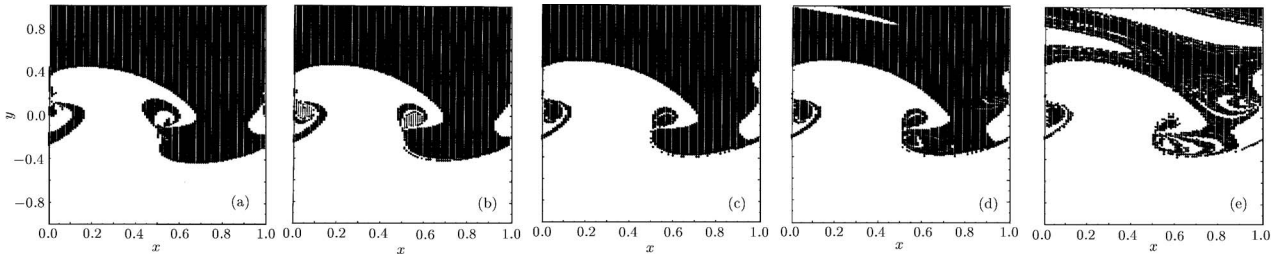

Fig. 3. Basins of attraction on the $x-y$ plane corresponding to the typical trajectories in Fig. 2 for: (a) $d_{\rm P}=3\times10^{-5}$ m; (b) $d_{\rm P}=7\times10^{-5}$ m (Besides the two local zones marked by thinner lines for the basin of period-1 orbit in the street, the global zone presents the basin for the period-1 orbit above the street.); (c) $d_{\rm P}=1\times10^{-4}$ m; (d) $d_{\rm P}=1.05\times10^{-4}$ m; (e) $d_{\rm P}=1.2\times10^{-4}$ m.

points attracted on the orbits. Concerning the stability of orbits, we take $x=0$ as a Poincaré section and determine their maximal Lyapunov exponents.[9] In Fig. 2(a), for $d_{\rm P}=3\times10^{-5}$ m, a period-1 orbit and all corresponding streamlines are drawn. The period-1 orbit, where the particles move from left to right, distributes above the street. In Fig. 4, for the period-1 orbit, the maximal Lyapunov exponent is -0.05, so the orbit is stable. In the motion of particles, points corresponding to those in the basin of attraction in Fig. 3(a) suspend on the period-1 orbit. At the same time, points corresponding to those outside the basin of attraction in Fig. 3(a) escape from the central region of flow. In Fig. 2(b), for $d_{\rm P}=7\times10^{-5}$ m, two period-1 orbits are placed above and in the street, respectively. On the orbit above the street, the particles move from left to right. In Fig. 4, the maximal Lyapunov exponent of the period-1 orbit is -0.17, so the orbit is stable. However, on the orbit in the street, the particles move in an opposite direction, i.e. from right to left. The maximal Lyapunov exponent of the period-1 orbit is -0.53, so the orbit is also stable. For the two period-1 orbits, the corresponding basins of attraction are plotted in Fig. 3(b). One is similar to that in Fig. 3(a), the other is distributed in two local zones. The basin for the orbit in the street is surrounded by that for the orbit above the street. In Fig. 2(c), for $d_{\rm P}=1\times10^{-4}$ m, a period-2 orbit, which distributes above the street, is drawn as a particle trajectory. On the orbit, the particles move from left to right. In Fig. 4, the maximal Lyapunov exponent of the period-2 orbit is -0.003, so the orbit is stable. The corresponding basin of attraction is plotted in Fig. 3(c). In the motion of particles, the points attracted on the period-2 orbit in Fig. 3(c) are less than those attracted on the period-1 orbit in Fig. 3(a). In Fig. 2(d), for $d_{\rm P}=1.05\times10^{-4}$ m, a period-4 orbit is drawn above the street. On the orbit, the particles move from left to right. In Fig. 4, the maximal Lyapunov exponent of the period-4 orbit is -0.02, so the orbit is stable. The corresponding basin of attraction is plotted in Fig. 3(d). The geometry of the basin is different from those in Figs. 3(a)–3(c). Some points near $y=1$ escape from the basin of attraction in the dispersion of particles. In Fig. 2(e), for $d_{\rm P}=1.2\times10^{-4}$ m, a quasi-periodic or chaotic orbit is drawn above the street. On the orbit, the particles move from left to right. In Fig. 4, the maximal Lyapunov exponent of the orbit is 0.51, so the orbit is chaotic. The corresponding basin of attraction is plotted in Fig. 3(e). The geometry of basin is similar to that in Fig. 3(d), but the escaped zone increases. The escaped points in Fig. 3(e) permeate into the basin of attraction in Fig. 3(d). From those examples, we can conclude that, along with the increases of particle size, more and more initial points distributed in the central region of flow escape. At the same time, the particle trajectories bifurcate from periodic orbits to chaotic orbits.

In order to explain the bifurcation phenomenon, we analyse the orders of magnitude of parameters in Eq. (3). To give physical values in the calculation, the parameters f_d and ϵ appear to be of the order of one and 10^{-4}, respectively. When d is taken as

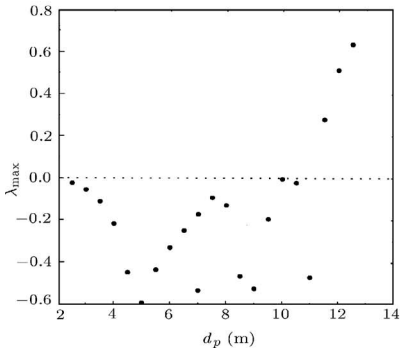

Fig. 4. Variation of the maximal Lyapunov exponent $\lambda_{\max}$ with d_{P}.

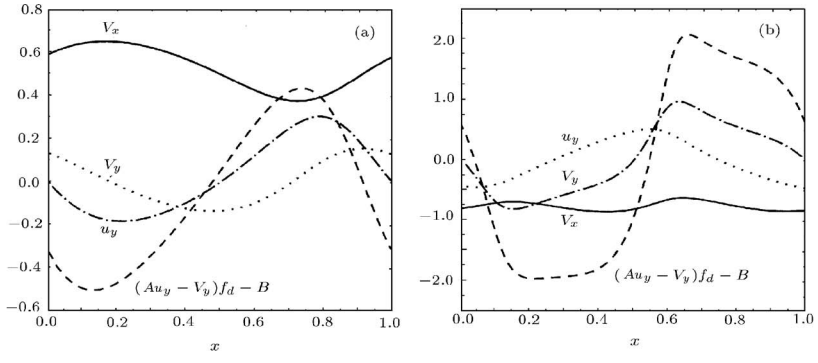

Fig. 5. Distribution of V_x, V_y, u_y and $(Au_y - V_y)f_d - B$ along x on the period-1 orbit (a) above the street; (b) in the street for $d_{\mathrm{P}} = 7 \times 10^{-5}$ m.

$10^{-5} - 10^{-4}$ m, the parameters T, A and B appear to be of the order 10^{-3} s $- 10^{-1}$ s, $10^{-1} - 1$ and $10^{-3} - 1$, respectively. In this case, Eq. (3) is dominated by the drag term $(A\boldsymbol{u} - \boldsymbol{V})f_d$ and the gravity term $B\boldsymbol{g}$. In Ref. [6], by considering the drag term, the essential dynamics takes place on the two-dimensional centre manifolds. To compare with the result, we find the bifurcation process disappearing when we eliminate the gravity term in Eq. (3). In the following, we take the attractors for $d_{\mathrm{P}} = 7 \times 10^{-5}$ m as an example to discuss their existence. In Fig. 5, we present the values of V_x, V_y, u_y and $(Au_y - V_y)f_d - B$ along the two period-1 orbits. For the period-1 orbit above the street, in Fig. 5(a), since $V_x > 0$ in $x \in [0, 1)$, the motional direction of particles is from left to right. Firstly, when a particle moves from $x = 0$ to $x = 0.475$, the negative term $(Au_y - V_y)f_d - B$ causes a decrease of V_y from 0.130 to -0.135. At the same time, it leads to an increase of the term $(Au_y - V_y)f_d - B$. Then, when the particle moves from $x = 0.475$ to $x = 0.914$, the positive term $(Au_y - V_y)f_d - B$ causes an increase of V_y from -0.135 to 0.157. At the same time, it leads to a decrease of the term $(Au_y - V_y)f_d - B$. Furthermore, when the particle moves from $x = 0.914$ to $x = 1$, the negative term $(Au_y - V_y)f_d - B$ causes a decrease of V_y from 0.157 to 0.130. At the same time, it leads to increase of the term $(Au_y - V_y)f_d - B$. According to the periodic boundary condition, when the particle reaches $x = 1$, it returns to $x = 0$. Therefore, the combination of the drag and gravity terms in the vertical direction has a periodic vibration along with the variation of the vertical velocity of particles and makes the period-1 orbit. In Fig. 5(b), for the period-1 orbit in the street, since $V_x < 0$ in $x \in [0, 1)$, the motional direction of particles is from right to left. In the same way as in Fig. 5(a), the term $(Au_y - V_y)f_d - B$ brings into a periodic vibration of particles and makes the period-1 orbit. From the above observation, we can conclude that the drag and gravity terms lead to the bifurcation behaviour in dilute particle dispersion. The direction of V_x and distribution of u_y determine the vertical position of attractors.

In summary, we have shown that in a Kármán vortex street flow, particle size influence dilute particle dispersion. Along with an increase of the particle size, a period-doubling bifurcation to a chaotic orbit emerges, as well as a decrease of the corresponding basins of attraction. A crisis leads the attractor to escape from the central region of flow. In the motion of dilute particles, the bifurcation phenomenon results from drag and gravity terms.

References

[1] Maxey M R and Riley J J 1983 *Phys. Fluids* **26** 883
[2] Chung J N and Troutt T R 1988 *J. Fluid Mech.* **186** 199
[3] Ganan-Calvo A M and Lasheras J C 1991 *Phys. Fluids* A **3** 1207
[4] Tio K-K, Ganan-Calvo A M and Lasheras J C 1993 *Phys. Fluids* A **5** 1679
[5] Tang L, Wen F, Yang Y, Crowe C T, Chung J N and Troutt T R 1992 *Phys. Fluids* A **4** 2244
[6] Burns T J, Davis R W and Moore E F 1999 *J. Fluid Mech.* **384** 1
[7] Clift R, Grace J R and Weber M E 1978 *Bubbles, Drops and Particles* (New York: Academic)
[8] Panton R L 1984 *Incompressible Flow* (New York: Wiley)
[9] Eckmann J P and Ruelle D 1985 *Rev. Mod. Phys.* **57** 617